Roughness of time series in a critical interface model

S. L. A. de Queiroz*
Instituto de Física, Universidade Federal do Rio de Janeiro, Caixa Postal 68528, 21941-972 Rio de Janeiro RJ, Brazil
(Received 18 May 2005; revised manuscript received 1 August 2005; published 5 December 2005)

We study roughness probability distribution functions (PDFs) of the time signal for a critical interface model, which is known to provide a good description of Barkhausen noise in soft ferromagnets. Starting with time "windows" of data collection much larger than the system's internal "loading time" (related to demagnetization effects), we show that the initial Gaussian shape of the PDF evolves into a double-peaked structure as window width decreases. We advance a plausible physical explanation for such a structure, which is broadly compatible with the observed numerical data. Connections to experiment are suggested.

DOI: 10.1103/PhysRevE.72.066104 PACS number(s): 05.65.+b, 05.40.−a, 75.60.Ej, 05.70.Ln

I. INTRODUCTION

The probability distribution functions (PDFs) of critical fluctuations in assorted systems have been the subject of much recent interest, mainly stemming from the realization that they exhibit a remarkable degree of universality [1–4].

The roughness w_2 of a fluctuating interface with N elements is the position-averaged square width of the interface height above an arbitrary reference level [4,5]:

$$w_2 = N^{-1}\sum_{i=1}^{N}(h_i - \bar{h})^2, \tag{1}$$

where $\bar{h}$ is the average interface height. The finite-size scaling of the first moment of the roughness PDF gives the roughness exponent ζ [6]:

$$\langle w_2(L)\rangle \sim L^{2\zeta}, \tag{2}$$

where angular brackets stand for averages over the ensemble of allowed interface configurations, and L is some finite linear dimension characterizing the system in study. The width PDF $P(w_2)$ for correlated systems at criticality may be put into a scaling form [3–5,7],

$$\Phi(z) = \langle w_2\rangle P(w_2), \quad z \equiv w_2/\langle w_2\rangle, \tag{3}$$

i.e., the scaling function $\Phi(z)$ is expected to depend only on the scaled width $w_2/\langle w_2\rangle$. In other words, the size dependence must appear exclusively through the average width $\langle w_2\rangle$. Comparison of experimental or simulational data to specific analytical forms, whose suitability to the description of the case at hand has been anticipated by physical arguments, usually results in good agreement. Thus the PDF of voltage fluctuations in semiconductor films was fitted very well by that of perfect Gaussian $1/f$ noise [3]; simulational data for the single-step model of deposition-evaporation, by the PDF of a random-walk process [7] (the latter corresponds to perfect Gaussian $1/f^2$ noise, or *Wiener process* [4]). Further progress was made possible via the analytical evaluation of roughness PDFs for generalized Gaussian noise with independent Fourier modes (i.e., $1/f^\alpha$ noise with general, continuously-varying α) [4]. Consideration of the scaling properties of height-height correlation functions and their Fourier transforms implies [5] that

$$\alpha = d + 2\zeta, \tag{4}$$

where d is the interface dimensionality and ζ is defined in Eq. (2). Equation (4) is valid provided that $\zeta > 0$ [4], i.e., $\alpha > 1$ in the present case where the "interface" is a time series (see below).

In previous work [8] we applied the ideas outlined above, to investigate the interface roughness PDFs of a single-interface model which has been used in the description of Barkhausen "noise" (BN) [9–12]. This is an intermittent phenomenon which reflects the dynamics of domain-wall motion in the central part of the hysteresis cycle in ferromagnetic materials (see Ref. [13] for an up-to-date review). By ramping an externally applied magnetic field, one causes sudden turnings (avalanches) of groups of spins. The consequent changes in magnetic flux induce a time-dependent electromotive force $V(t)$ on a coil wrapped around the sample. Analysis of $V(t)$, assisted by suitable theoretical modeling, provides insight into both the domain structure itself and its dynamical behavior. It has been proposed that BN is an illustration of "self-organized criticality" [9,14–16], in the sense that a broad distribution of scales (i.e., avalanche sizes) is found within a wide range of variation of the external parameter, namely the applied magnetic field, without any fine-tuning. The interface model studied here [9] incorporates a self-regulating mechanism, in the form of a demagnetization factor.

We have shown [8] that the demagnetizing term is irrelevant as regards interface roughness distributions, with the conclusion that in this respect the behavior of self-regulated systems is in the same universality class as that of the quenched Edwards-Wilkinson model [17–20], at criticality (i.e., at the interface depinning transition).

However, when one considers the time series of intermittent events which characterizes BN, it is known that the demagnetizing term is responsible for the introduction of short-time negative correlations in the model (such correlations are observed in experiments as well) [9]. The question then arises of whether a corresponding signature of self-regulation will be present when the roughness distribution of the time

*Electronic address: sldq@if.ufrj.br

sequence of BN events is examined. Since the traditional data acquisition method in the study of BN is exactly via the time series of induced voltages, an investigation along these lines may establish useful connections between observational data and the basic physical mechanisms underlying BN.

II. MODEL INGREDIENTS AND DYNAMICS

We use the single-interface model introduced in Ref. [9] for the description of BN. In line with experimental procedure, the external field H acting on the sample is assumed to increase linearly in time, therefore its value is a measure of "time." We consider the adiabatic limit of a very slow driving rate, thus avalanches are considered to be instantaneous (occurring at a fixed value of the external field). In this simplified version, a plot of $V(t)$ against t consists of a series of spikes of varying sizes, placed at nonuniform intervals. Generalizations for a finite driving rate may be devised [11,21,22], but will not concern us here.

Simulations are performed on an $L_x \times L_y \times \infty$ geometry, with the interface motion set along the infinite direction. Since we are interested in fluctuations of the Barkhausen signal in *time*, we keep geometric aspects at the simplest level, i.e., $L_y=1$ (system dimensionality $d=2$, interface dimensionality $d'=1$). Periodic boundary conditions are imposed at $x=0,L$.

The interface (180-degree domain wall separating spins parallel to the external field from those antiparallel to it) is composed by L discrete elements whose x coordinates are $x_i=i$, $i=1,\ldots,L$, and whose (variable) heights above an arbitrary reference level are h_i. The simulation starts with a flat wall: $h_i=0$ for all i.

Each element i of the interface experiences a force given by

$$f_i = u(x_i,h_i) + k[h_{i+1} + h_{i-1} - 2h_i] + H_e, \tag{5}$$

where

$$H_e = H - \eta M. \tag{6}$$

The first term on the right-hand side (RHS) of Eq. (5) represents quenched disorder, and is drawn from a Gaussian distribution of zero mean and width R; the intensity of surface tension is set by k, and the effective field H_e is the sum of a time-varying, spatially uniform, external field H and a demagnetizing field which is taken to be proportional to $M = (1/L)\Sigma_{i=1}^{L} h_i$, the magnetization (per site) of the previously flipped spins for a lattice of transverse width L. Here we use $R=5.0$, $k=1$, $\eta=0.005$, values for which fairly broad distributions of avalanche sizes are obtained [8,10–12].

The dynamics goes as follows. For fixed H, starting from zero, the sites are examined sequentially; at those for which $f_i>0$, h_i is increased by one unit, with M being updated accordingly; the corresponding new value of u is drawn. The whole interface is swept as many times as necessary, until only sites with $f_i<0$ are left, which marks the end of an avalanche. The external field is then increased until $f_i=0$ for at least one site. This is the threshold of a new avalanche, which is triggered by the update of the site(s) with $f_i=0$, and so on.

The effect of the demagnetizing term on the effective field H_e is that at first it rises linearly with the applied field H, and then, upon further increase in H, saturates (apart from small fluctuations) at a value rather close to the critical external field for the corresponding model *without* demagnetization [9,10].

III. TIME SERIES: CORRELATIONS AND ROUGHNESS

As explained above, owing to the assumed linear increase of applied field with time (in analogy with experimental setups), we shall express time in units of H as given in Eqs. (5) and (6). We have generated time series of BN, with $O(10^4-10^5)$ events. Steady state, i.e., the stabilization of H_e of Eq. (6) against external field H, occurs after some 200 events, for the range of parameters used here. Though we used only steady-state data, it was noted that inclusion of those from the transient does not appreciably distort any of the quantities studied.

In experiment, the integrated signal $\int_{\Delta t} V(t)dt$ is proportional to the magnetization change (number of upturned spins) during the interval Δt. In the adiabatic approximation used here, a boxlike shape is implicitly assumed for each avalanche (i.e., details of the internal structure of each peak, as it develops in time, are ignored, on acount of its duration being very short), thus the instantaneous signal intensity (spike height) is proportional to the corresponding avalanche size.

We sample the fluctuations of the signal along successive "windows" of equal time duration W, each containing many spikes. Each window is divided into equally-spaced bins of size δ; the signal intensity associated to each bin is the sum of the sizes of all avalanches which occurred within that bin. The roughness w_2 of the signal on a given window starting, say, at $t=0$, is given by

$$w_2 = \frac{1}{W/\delta}\sum_{i=1}^{W/\delta} (V_i - \bar{V})^2, \quad V_i = \sum_{t\in[(i-1)\delta, i\delta]} V(t), \tag{7}$$

where $\bar{V}$ is an average of $V(t)$ over the whole window span W.

As the signal is intermittent, there are significant periods (waiting times, henceforth referred to as WT) of no activity at all. Such quiet intervals must be properly accounted for in the statistics of fluctuations, hence care must be taken when setting up the bin size δ.

We have examined WT distributions, for varying lattice widths $L=200,400,800$. In Fig. 1 (lower curve) we display a double-logarithmic plot of the probability of occurrence of assorted WTs for $L=400$, against WT, sampled over 8×10^6 events. The distribution is generally rather flat, apart from (i) a sharp cutoff at the high end (related to the finite cutoff in the avalanche size probability distribution, see the discussion of loading times below), and (ii) a number of peaks concentrated in a somewhat narrow region corresponding to $10^{-5} \lesssim \mathrm{WT} \lesssim 10^{-4}$. The latter are associated to very frequent and small, spatially localized (i.e., noncritical) events involving typically $N=1-10$ sites [11]. This is easy to see by recalling from Eqs. (5) and (6) that, since the demag-

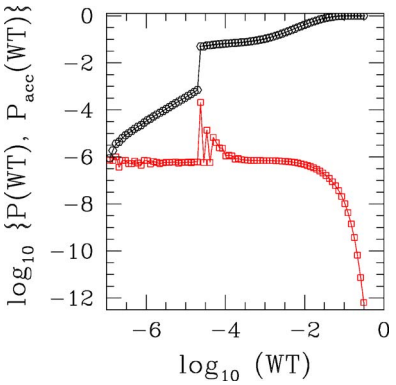

FIG. 1. (Color online) Double-logarithmic plot of probability distribution, $P(\mathrm{WT})$, of waiting times (lower curve), and accumulated distribution, $P_{\mathrm{acc}}(\mathrm{WT}) \equiv \int_0^{\mathrm{WT}} P(t)dt$ (upper curve). $L=400$.

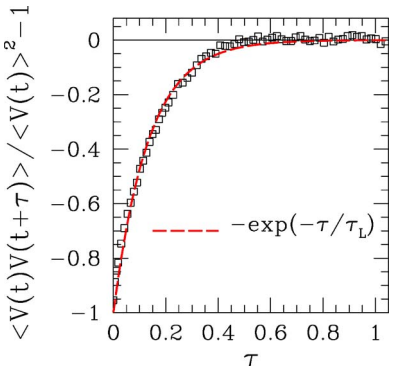

FIG. 2. (Color online) Normalized two-time correlations (averaged over t) $\langle V(t)V(t+\tau)\rangle/\langle V(t)\rangle^2-1$ for system with $L=400$. Dashed line is fit of data to single-exponential form, from which $\tau_L=0.14(1)$.

netization term keeps H_e approximately constant, a small avalanche with N spins overturned decreases the internal field by $\eta N/L$, thus requiring approximately the same increase in external field in order to bring the system back to criticality. We have checked that the peaks move consistently with this argument, i.e., their horizontal position is shifted leftward by a factor of $\log_{10} 2$ for each doubling of L.

Upon consideration of integrated WT distributions (upper curve in Fig. 1), we decided to set the bin size $\delta=10^{-5}$ (for $L=400$, the system size for which most of our calculations are done, see below). With such a choice, WTs shorter than δ occur with less than 1% frequency. This ensures both that inactive periods are not wrongly obscured by bursts of activity, and that consecutive avalanches are rather unlikely to be lumped together.

At this point, a comment must be made on the connection of the above results with previous investigations of WT distributions in BN. In Ref. [23] it was predicted, from a fractal analysis of the ABBM [24] model which describes domain-wall motion via a Langevin equation, that $P(\mathrm{WT}) \sim (\mathrm{WT})^{-(2-c)}$, where c is proportional to the external field driving rate. Experimental data in SiFe samples are consistent with this [23]. The present case of adiabatic driving would then correspond to $c \to 0$. However, it is crucial in the analysis of Ref. [23] that the BN pulse durations be finite (even though they shorten accordingly in the $c \to 0$ limit). Indeed, the result just quoted relies on considering the properties of complementary sets, both with nonzero fractal dimension (namely the time intervals during which there is domain-wall motion, versus those of no activity, i.e., WTs). The approximation used here, of considering BN pulses as having exactly zero duration, destroys the connection of our data with the conceptual framework in which the power-law dependence $P(\mathrm{WT}) \sim (\mathrm{WT})^{-(2-c)}$ was found. Though in this sense the flat WT distribution found here is most likely an artifact of the model, the conclusions extracted from the distribution with respect to the choice of δ remain valid.

We now turn to the choice of window width W. Recall that real-space properties, e.g., interface roughness, of the systems under study benefit from divergence of the system's natural length scale, as it self-tunes its behavior to lie close to a second-order (depinning) transition [8]. For such quantities, universality ideas apply, so one expects finite-lattice effects to be present only as an overall scale factor, e.g., $\langle w_2 \rangle$ in Eq. (3) [3–5,7]. However, in the study of time series for the same systems, one must bear in mind that a finite time scale τ_L ("loading time") is introduced via the demagnetization term [9]. This is illustrated in Fig. 2 (similar plots, exhibiting both simulational and experimental results, can be found in Ref. [9]) where normalized two-time correlations $\langle V(t)V(t+\tau)\rangle/\langle V(t)\rangle^2-1$ (averaged over t) are shown. Therefore, different regimes will be found, depending on the value of $x \equiv W/\tau_L$. The limit $x \gg 1$ is expected to reproduce the white noise characteristic of uncorrelated fluctuations, for which the roughness distribution is a pure Gaussian. On the other hand, non-trivial effects may arise for $x \sim 1$.

Before going further, it must be remarked that τ_L in fact decreases for increasing L. This can be understood by recalling that (i) the probability distribution for avalanche size s goes roughly as $P(s) \sim s^{-a} \exp(-s/s_0)$ [9–12]; (ii) the cutoff s_0 scales approximately as $s_0 \sim L^{0.8}$ in the present case of a one-dimensional interface [10]. Thus the maximum waiting time τ_M will vary as $\tau_M = \eta s_0/L \sim L^{-0.2}$. For $L=400$, we find $s_0 \simeq 4 \times 10^4$ [12], which explains both the sharp drop in the WT distribution at $\mathrm{WT} \simeq 0.5$ in Fig. 1, and the complete vanishing of correlations at $\tau \gtrsim 0.5$ in Fig. 2.

In BN studies the connection between lattice-size-dependent quantities in simulations, and their experimental counterparts, becomes especially clear when one considers the L-dependent cutoff in the power-law avalanche size distribution, and its relationship to the maximum domain size in magnetic samples [10]. In the present case it should be stressed that finite loading times are measured in experiment, under suitable conditions [9]. Thus, we assume that the loading times found here are not simply a finite-size artifact of simulations, bound to vanish in the thermodynamic limit characteristic of real systems. Instead, although we are not in a position to propose quantitative comparisons, they must correspond to the experimentally observed ones.

IV. RESULTS

By generating many realizations of the roughness w_2 defined in Eq. (7) for given values of the physical parameters,

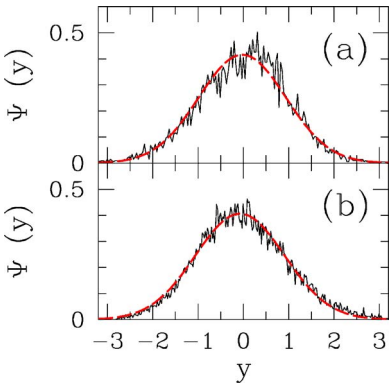

FIG. 3. (Color online) Scaled roughness distributions $\Psi(y)$ of time series, for y of Eq. (8). $L=400$; window width $W=100$. (a) Demagnetizing factor $\eta=0.005$ ($\tau_L \simeq 0.14$), 6×10^3 samples. Dashed line is Gaussian fit to data with mean at $y=0.04(1)$, width $\sigma=0.96(1)$. (b) Demagnetizing factor $\eta=0$ (see text), 2.1×10^4 samples. Dashed line is Gaussian fit to data, with mean at $y=-0.07(1)$, width $\sigma=0.98(1)$.

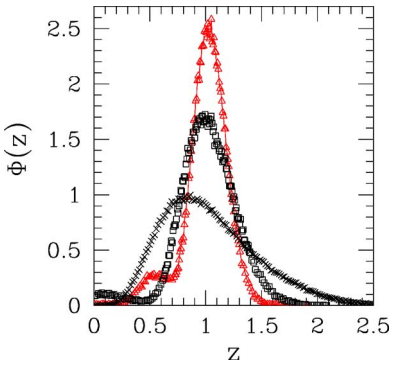

FIG. 4. (Color online) Scaled roughness distributions $\Phi(z)$ of time series, for z of Eq. (3). $L=400$. Window width $W=10$ (triangles, 1.2×10^5 samples), 2.5 (squares, 1.2×10^5 samples), and 1.0 (crosses, 5.7×10^5 samples).

we have obtained the corresponding roughness PDFs. The shapes of roughness PDFs found here do not usually conform to the generalized Gaussian ($1/f^{\alpha}$) distributions introduced in Ref. [4], although they display certain similarities to the pure Gaussian limit, which corresponds to $\alpha=1/2$ in the scheme of Ref. [4]. We have found it convenient to adhere to conventions used in that Reference and related work, namely expressing the PDFs in a scaling form, see Eq. (3).

We first examine the limit $x \gg 1$. Similarly to $1/f^{\alpha}$ PDFs with $\alpha \leqslant 1$ [4], our results in this limit approach a δ-function shape when expressed in terms of z of Eq. (3). The solution, pointed out in Refs. [3,4], is to use scaling by the variance, instead of by the average, i.e., switch to the variable

$$y = \frac{w_2 - \langle w_2 \rangle}{\sqrt{\langle w_2^2 \rangle - \langle w_2 \rangle^2}}. \tag{8}$$

The corresponding scaling function will be denoted by $\Psi(y)$.

In Fig. 3 we show results for window width $W=100$, in terms of y of Eq. (8). While in (a) the demagnetizing factor is $\eta=0.005$ (thus $\tau_L \simeq 0.14$ from Fig. 2), the data in (b) correspond to simulations of the same system, with $\eta=0$. As explained in Ref. [8], in this case the system is kept close to criticality by the following procedure. We first determined the approximate critical value H_e^c of the internal field H_e of Eq. (6), by starting a simulation with $\eta \neq 0$ and waiting for H_e to stabilize. At that point, we set $\eta=0$ and repeatedly swept H in the interval $(\gamma H_e^c, H_e^c)$, $\gamma \lesssim 1$, according to the procedure delineated in Sec. II. We have used $\gamma=0.9$ for the data displayed in Fig. 3(b). With $H_e^c \simeq 5.4$ for the disorder and elasticity parameters used here, data corresponding to a window of "width" $W=100$ in this case was in fact given by the collation of data from $\sim W/(1-\gamma)H_e^c = 185$ consecutive field sweeps as just described. Note that, within a given field sweep, many noncritical events are thus sampled (which would by themselves give rise to a nonuniversal PDF, see below the discussion for narrow windows). However, owing to the central limit theorem, the result of the collation of many independent segments should yield an overall behavior which is essentially Gaussian.

One can see that in both cases, a single Gaussian centered at $y \simeq 0$ and with variance $\simeq 1$ gives a good fit to data, confirming our expectation that demagnetization-induced correlations would be essentially washed away for $W \gg \tau_L$. It is worth mentioning, however, that the *unscaled* variables tell a slightly different story: for the data of Fig. 3(a) one has $\langle w_2 \rangle \pm \sigma = (127 \pm 6) \times 10^3$, while in (b) $\langle w_2 \rangle \pm \sigma = (6.3 \pm 2.2) \times 10^3$. Clearly, our data would approach a δ-function shape if plotted in terms of z defined in Eq. (3).

Considering now narrower windows, and keeping the demagnetizing factor $\eta=0.005$, we show data for $W=10.0$, 2.5, and 1.0 in Fig. 4, where we have reverted to plotting our results in terms of the variable z defined in Eq. (3). This is because it was noticed that, against diminishing x, the scaled roughness PDFs followed a trend away from the δ-function shape which was the motivation for using the variable y of Eq. (8). In order to produce an accurate picture of deviations from the Gaussian limit, we have generated a much larger number of samples [$O(10^5)$] than for $W=100$.

Before analyzing the shapes exhibited in Fig. 4, it is instructive to check how the demagnetization term influences the roughness PDFs in the narrow-window limit. In Fig. 5 the scaled distributions for $W=10$ are shown, both with and without demagnetization. The shapes of PDFs are clearly rather distinct from each other, highlighting the relevance of demagnetization effects in this limit. For $\eta=0$ the distribution peaks at $z \simeq 0.15$ and decays very slowly afterwards. As mentioned above in connection with the data of Fig. 3(b), this reflects the nonuniversal statistics of noncritical events which our calculational method for $\eta=0$ inevitably includes. The difference relative to that case is that for $W=10$, each roughness sample is the collation of only ~ 19 consecutive field sweeps. The corresponding results show that, in contrast to $W=100$, here one is outside the range of applicability of the central limit theorem.

From now on we shall only deal with $\eta \neq 0$. Even though $W=10.0$ corresponds to $x \simeq 70$, it is clear from Fig. 4 that a secondary peak is evolving, i.e., a significant distinction is emerging with respect to the simple Gaussian picture found

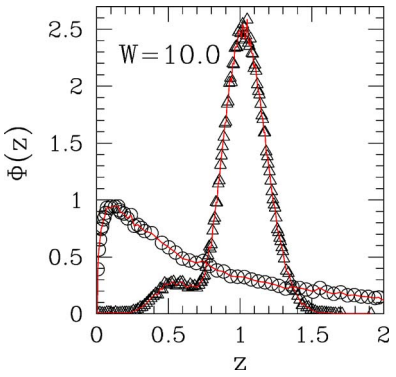

FIG. 5. (Color online) Scaled roughness distributions $\Phi(z)$ of time series, for z of Eq. (3), with and without demagnetization. $L=400$; window width $W=10$. Triangles, $\eta=0.005$, 1.2×10^5 samples; circles, $\eta=0$, 2.1×10^5 samples.

for larger W. Data for $W=5.0$ (not shown) are virtually identical to those for $W=10.0$. While a secondary peak still shows up for $W=2.5$, data for $W=1.0$ display only a single maximum (however, these latter clearly differ from a pure Gaussian).

We then attempted to fit the data in Fig. 4 to analytical forms. The $W=10.0$ results strongly suggest a double-Gaussian ansatz, as

$$\Phi(z) = bG_1(z) + (1-b)G_2(z), \tag{9}$$

where G_i is a Gaussian centered at a_i with variance σ_i^2. As W grows, one would expect $b\to1$, $a_1\to1$ in Eq. (9). Data for $W=10.0$ are well fitted by $b=0.924(2)$, $a_1=1.03(1)$, $a_2=0.51(1)$, as seen in Fig. 6. The χ^2 per degree of freedom (χ^2_{DOF}) is 1.5×10^{-3}, indicating that the form Eq. (9) indeed provides a satisfactory description of simulational results in this case.

We have found that a similar fit, albeit of somewhat reduced quality [$\chi^2_{\mathrm{DOF}}=3\times10^{-3}$, with $b=0.955(5)$, $a_1=1.02(1)$, $a_2=0.06(3)$] is feasible for the $W=2.5$ data as well. Turning to $W=1.0$, the double-Gaussian ansatz worked surprisingly well, producing $\chi^2_{\mathrm{DOF}}=6\times10^{-4}$, with $b=0.53(5)$, $a_1=1.24(4)$, $a_2=0.77(1)$ (i.e., the two curves are roughly symmetric about $z=1$, with approximately equal weights).

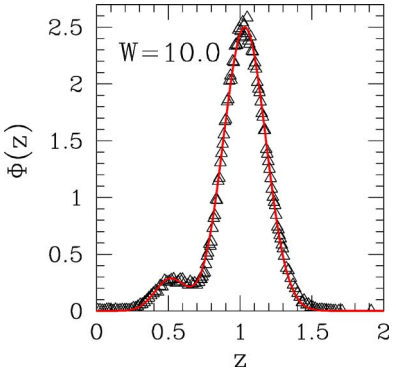

FIG. 6. (Color online) Scaled roughness distribution $\Phi(z)$ of time series, for z of Eq. (3). $L=400$. Window width $W=10$. Triangles are simulational data. Thick line is fit to Eq. (9), with $b=0.924(2)$, $a_1=1.03(1)$, and $a_2=0.51(1)$. $\chi^2_{\mathrm{DOF}}=1.5\times10^{-3}$.

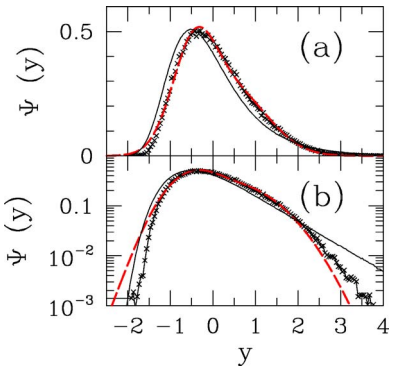

FIG. 7. (Color online) Crosses: scaled roughness distribution $\Psi(y)$ of time series, for y of Eq. (8). $L=400$; window width $W=1$. Dashed line is double-Gaussian fit to data [Eq. (9)]. Full line is Fisher-Tippet-Gumbel distribution with window boundary conditions. Vertical axis is linear in (a), logarithmic in (b).

Given that a double-peak structure is far from obvious for the $W=1.0$ data, alternative forms must be considered which might also provide a suitable fit to data in this limit. We investigated the family of roughness PDFs for $1/f^\alpha$ noise [4,5], keeping in mind that window boundary conditions (WBC) are the appropriate ones in this case [3–5,8,25]. Such PDFs are usually available in closed form [25]. However, close to $\alpha=1$ it is more time-efficient to evaluate PDFs numerically via the usual procedure of first generating a very long sequence of Gaussian white noise, Fourier-transforming that sequence, multiplying the Fourier components by $f^{-\alpha/2}$ and then inverting the Fourier transform [3,4]. The resulting sequence is pure $1/f^\alpha$ noise, which is then chopped into windows for analysis of the corresponding roughness PDF.

The best fit of the $1/f^\alpha$ family to our data was achieved for $\alpha=1$, that is, the Fisher-Tippet-Gumbel (FTG) statistics of extremes [3]. Even so, significant discrepancies remain. The overall picture is illustrated in Fig. 7, where we have switched again to the variable y of Eq. (8) because the FTG curve is better visualized in this way [3,4]. One sees that, even though the double-Gaussian curve gives an excellent fit in the central area of the plot where $\Psi(y)\gtrsim0.1$, it fails away from there, especially at the lower end. As to the FTG curve, while it follows the data closely, it never actually matches them.

V. DISCUSSION AND CONCLUSIONS

The usual approach to the frequency domain in BN literature is via the study of power spectra [13,26]. It has been found [11] that, in the adiabatic limit of the interface model under consideration here, the power spectrum behaves approximately as $1/f^2$ within an intermediate range of frequencies. One might construe this as indicating that the pure $1/f^2$ noise model of a Wiener process [4,7] applies in this case. However, the numerically-obtained full roughness PDF, which contains much more information than a section of the power spectrum, tells a more nuanced story. Indeed, in gen-

eral it does not follow a shape close to that of $1/f^{\alpha}$ curves, except for narrow windows. Even there, the closest fit within that family is for $\alpha \simeq 1$.

The question then arises of whether the generalized Gaussian approximation underlying $1/f^{\alpha}$ noise models, in which the Fourier modes are considered as uncorrelated [4], is suitable for the description of BN time series. Our results, when considered in their evolution as window width varies, appear more consistent with the idea that the similarity of our PDFs to that of $1/f$ noise, found at the narrow-window limit, is fortuitous. We recall that, even in studies of real-space interface roughness, it is known that the independent-mode approximation gives rise to small but systematic discrepancies against experimental data, which can be traced back to higher cumulants of the correlation functions [5]. Furthermore, even more severe discrepancies have been found when boundary conditions other than periodic (e.g., window, as is the case here) are considered [8,27].

Turning now to the double-Gaussian picture, admittedly phenomenological in its inspiration, nonetheless it gives a description which is both numerically closer to actual data, and spans a broad range of window widths.

The physical origins of the double-peak structure may be traced back to the demagnetization term, and the consequent negative correlations illustrated in Fig. 2. A window of width W contains at least W/τ_M segments whose internal roughness profiles are uncorrelated to each other. On the other hand, within each such segment, negative correlations are significant at least to some extent, thus preventing fluctuations from becoming very large. This latter effect gives rise to the secondary peaks at $y<0$, or equivalently, $z<1$. With $\tau_L \simeq 0.14$, $\tau_M \simeq 0.5$ for the $L=400$ systems which have been the focus of our study, one has for $W=1$ that both inter- and intrasegment fluctuations have similar weights, hence the $b \simeq 0.5$ result for the double-Gaussian fit in that case. For $W/\tau_M \gg 1$ the dominant picture is one of many uncorrelated "blobs" of length $\sim \tau_M$, yielding the effective single-Gaussian limit observed.

The double-Gaussian picture displays features which are not fully understood at present. Figure 8 exhibits the variation of parameters b, a_1, and a_2 of Eq. (9) against W for not very large window widths (in addition to $W=1.0$, 2.5, 5.0, and 10.0 we ran simulations at $W=0.5$ and 1.5). While b varies approximately as expected within this theoretical framework (albeit with small nonmonotonicities), and a_1 follows a rather monotonic trend, the behavior of a_2 is intriguing, showing an apparent trend reversal. So far we have not able to provide an explanation for this.

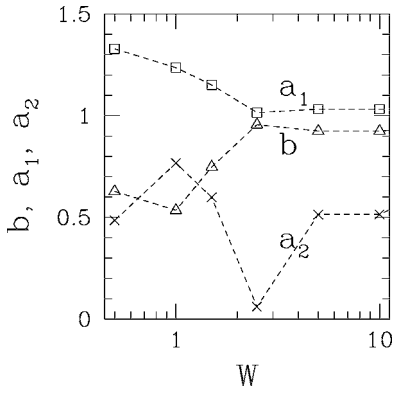

FIG. 8. Fitting parameters b (triangles), a_1 (squares), and a_2 (crosses) of double-Gaussian ansatz of Eq. (9), against window width W, for $W=0.5$, 1.0, 1.5, 2.5, 5.0, and 10. $L=400$.

An alternative explanation for the observed behavior at $W \simeq 1$ may be proposed, following a line similar to that advanced for the evolution of $\eta=0$ data with increasing W (see Fig. 5 and the respective discussion). In this scenario, the $W \simeq 1$ PDF shapes would be nonuniversal (i.e., neither $1/f^{\alpha}$ nor double-Gaussian). For larger $W \lesssim 10$ the central limit theorem would imply that, for the superposition of many (almost) decorrelated non-universal profiles, effective Gaussian structures should emerge. In this view, the peak at $z<1$ would again be ascribed to segments within which negative correlations are felt, with the peak at larger z corresponding to intersegment profiles.

Whatever the explanation of the behavior of roughness PDFs for $W \sim 1$, the extent of window widths for which an effectively double-peaked structure shows up is considerably larger than, say, τ_L. Thus, a fairly straightforward way to detect the presence of demagnetization effects in experimental setups would be via the analysis of roughness PDFs of the induced signal $V(t)$. Considering, e.g., the conditions for the Perminvar samples described in Ref. [9], where the average spacing between peaks is 13 msec and $\tau_M \simeq 200$ msec, analysis of windows of width ~ 2 sec should produce a well-defined double-peaked structure similar to that of Fig. 6.

ACKNOWLEDGMENTS

This research was partially supported by the Brazilian agencies CNPq (Grant No. 30.0003/2003-0), FAPERJ (Grant No. E26-152.195/2002), FUJB-UFRJ and Instituto do Milênio de Nanociências-CNPq.

[1] S. T. Bramwell, P. C. W. Holdsworth, and J.-F. Pinton, Nature (London) **396**, 552 (1998).

[2] S. T. Bramwell, K. Christensen, J.-Y. Fortin, P. C. W. Holdsworth, H. J. Jensen, S. Lise, J. M. López, M. Nicodemi, J.-F. Pinton, and M. Sellitto, Phys. Rev. Lett. **84**, 3744 (2000).

[3] T. Antal, M. Droz, G. Györgyi, and Z. Rácz, Phys. Rev. Lett. **87**, 240601 (2001).

[4] T. Antal, M. Droz, G. Györgyi, and Z. Rácz, Phys. Rev. E **65**, 046140 (2002).

[5] A. Rosso, W. Krauth, P. LeDoussal, J. Vannimenus, and K. J. Wiese, Phys. Rev. E **68**, 036128 (2003).

[6] A.-L. Barábasi and H. E. Stanley, *Fractal Concepts in Surface Growth* (Cambridge University Press, Cambridge, UK, 1995).

[7] G. Foltin, K. Oerding, Z. Rácz, R. L. Workman, and R. K. P.

Zia, Phys. Rev. E **50**, R639 (1994).
[8] S. L. A. de Queiroz, Phys. Rev. E **71**, 016134 (2005).
[9] J. S. Urbach, R. C. Madison, and J. T. Markert, Phys. Rev. Lett. **75**, 276 (1995).
[10] M. Bahiana, B. Koiller, S. L. A. de Queiroz, J. C. Denardin, and R. L. Sommer, Phys. Rev. E **59**, 3884 (1999).
[11] S. L. A. de Queiroz and M. Bahiana, Phys. Rev. E **64**, 066127 (2001).
[12] S. L. A. de Queiroz, Phys. Rev. E **69**, 026126 (2004).
[13] G. Durin and S. Zapperi, in *The Science of Hysteresis*, edited by G. Bertotti and I. Mayergoyz (Academic, New York, 2005).
[14] K. L. Babcock and R. M. Westervelt, Phys. Rev. Lett. **64**, 2168 (1990).
[15] P. J. Cote and L. V. Meisel, Phys. Rev. Lett. **67**, 1334 (1991).
[16] K. P. O'Brien and M. B. Weissman, Phys. Rev. E **50**, 3446 (1994).
[17] H. Leschhorn, Physica A **195**, 324 (1993).
[18] H. A. Makse and L. A. N. Amaral, Europhys. Lett. **31**, 379 (1995).
[19] H. A. Makse, S. Buldyrev, H. Leschhorn, and H. E. Stanley, Europhys. Lett. **41**, 251 (1998).
[20] A. Rosso, A. K. Hartmann, and W. Krauth, Phys. Rev. E **67**, 021602 (2003).
[21] B. Tadić, Physica A **270**, 125 (1999).
[22] R. A. White and K. A. Dahmen, Phys. Rev. Lett. **91**, 085702 (2003).
[23] G. Durin, G. Bertotti, and A. Magni, Fractals **3**, 351 (1995).
[24] B. Alessandro, C. Beatrice, G. Bertotti, and A. Montorsi, J. Appl. Phys. **68**, 2901 (1990).
[25] S. Moulinet, A. Rosso, W. Krauth, and E. Rolley, Phys. Rev. E **69**, 035103(R) (2004).
[26] M. C. Kuntz and J. P. Sethna, Phys. Rev. B **62**, 11 699 (2000).
[27] A. Rosso, R. Santachiara, and W. Krauth, cond-mat/0503134.